Understanding the thermal and mechanical stabilities of olivine-type $LiMPO_4$ (M=Fe, Mn) as cathode materials for rechargeable lithium batteries from first-principles

Ying Xie [a]*, Hai-Tao Yu [a], Ting-Feng Yi [a,b]*, Yan-Rong Zhu [b]

[a] *Key Laboratory of Functional Inorganic Material Chemistry (Heilongjiang University) , Ministry of Education, School of Chemistry and Materials Science, Heilongjiang University, Harbin 150080, PR China*

[b] *School of Chemistry and Chemical Engineering, Anhui University of Technology, Maanshan, Anhui 243002, PR China*

Corresponding Author

*E-mail: xieying@hlju.edu.cn (Dr. Ying Xie); tfyihit@163.com (Dr. Ting-Feng Yi).

Tel.: +86 -555 2311807. Fax: +86 555 2311552

Supporting informations

Theoretical details for calculating the Gibbs formation energies from elements ($\Delta_f G_{m,el.}$) or from oxides ($\Delta_r G_{m,ox.}$).

(1) Gibbs formation energies from elements ($\Delta_f G_{m,el.}$).

To evaluate the Gibbs formation energies ($\Delta_f G_{m,el}$) of $LiMPO_4$ (M=Fe, Mn) cathode materials from element phases, the molar Gibbs free energies of reactions ($\Delta_r G_m$) were calculated first. The molar Gibbs free energies of reactions ($\Delta_r G_m$) are directly related to the chemical reactions and can be derived from the energies of reactants and products. The thermodynamic cycles are described below,

$$\mathrm{Li(s, } I_{m-3m}) + \mathrm{FePO_4(s, } P_{3121}) \rightarrow \mathrm{LiFePO_4\ (s, } P_{nma}) \quad (1)$$

$$Li\left(s, I_{m-3m}\right) + FePO_4\left(s, P_{3121}\right) + Mn\left(s, F_{m-3m}\right) \rightarrow LiMnPO_4\left(s, P_{nma}\right) + Fe\left(s, I_{m-3m}\right) \quad (2)$$

As the entropy change and volume effect of solid materials are usually small and can be neglacted, $\Delta_r G_m$ (Eq.(1)) and $\Delta_r G_m$ (Eq.(2)) can be obtained approximately by,

$$\Delta_r G_m\left(Eq.(1)\right) = E\left(LiFePO_4\right) - E\left(Li\right) - E\left(FePO_4\right) \quad (3)$$

$$\Delta_r G_m(\mathrm{Eq.(2)}) = E(\mathrm{LiMnPO_4}) + E(\mathrm{Fe}) - E(\mathrm{Mn}) - E(\mathrm{Li}) - E(\mathrm{FePO_4}) \quad (4)$$

Furthermore, because the Gibbs free energy of reactions can be alternatively deduced from the Gibbs formation energies of substances, Eq. (3) and Eq. (4) can also be rewritten as,

$$\Delta_r G_m(\mathrm{Eq.(1)}) = \Delta_f G_m(\mathrm{LiFePO_4}) - \Delta_f G_m(\mathrm{Li}) - \Delta_f G_m(\mathrm{FePO_4}) \quad (5)$$

$$\Delta_r G_m(\mathrm{Eq.(2)}) = \Delta_f G_m(\mathrm{LiMnPO_4}) + \Delta_f G_m(\mathrm{Fe}) - \Delta_f G_m(\mathrm{Mn}) - \Delta_f G_m(\mathrm{Li}) - \Delta_f G_m(\mathrm{FePO_4}) \quad (6)$$

According to the available Gibbs formation energies of substances (See Table S1), $\Delta_f G_{m,el}(\mathrm{LiFePO_4})$ and $\Delta_f G_{m,el}(\mathrm{LiMnPO_4})$ can be determined. Furthermore, on the basis of similar algorithms, the Gibbs formation energies of $FePO_4$ (P_{nma}) and $MnPO_4$ (P_{nma}) from elements can also be derived, and the relevant reactions are

described as follows,

$$\mathrm{FePO_4(s, P_{3121}) \rightarrow\ FePO_4\ (s, P_{nma})} \quad (7)$$

$$FePO_4\left(s, P_{3121}\right) + Mn\left(s, F_{m-3m}\right) \rightarrow MnPO_4\left(s, P_{nma}\right) + Fe\left(s, I_{m-3m}\right) \quad (8)$$

For $LiMO_2$ ($R_{\bar{3}m}$), MO_2 ($R_{\bar{3}m}$), $LiMn_2O_4$ ($F_{d\bar{3}m}$), and Mn_2O_4 ($F_{d\bar{3}m}$) electrode materials, the experimental reaction pathways were considered[1-3],

$$\mathrm{Li_2O(s, F_{m\bar{3}m}) + 2CoO(s, F_{m\bar{3}m}) + \frac{1}{2}O_2(g) \xrightarrow{reaction} 2LiCoO_2(s, R_{\bar{3}m})} \quad (9)$$

$$\mathrm{Li_2O(s, F_{m\bar{3}m}) + 2NiO(s, F_{m\bar{3}m}) + \frac{1}{2}O_2(g) \xrightarrow{reaction} 2LiNiO_2(s, R_{\bar{3}m})} \quad (10)$$

$$\mathrm{CoO(s, F_{m\bar{3}m}) + \frac{1}{2}O_2(g) \xrightarrow{reaction} CoO_2(s, R_{\bar{3}m})} \quad (11)$$

$$\mathrm{NiO(s, F_{m\bar{3}m}) + \frac{1}{2}O_2(g) \xrightarrow{reaction} NiO_2(s, R_{\bar{3}m})} \quad (12)$$

$$\mathrm{Li_2O(s, F_{m\bar{3}m}) + 2MnO_2\left(s, P_{42/mnm}\right) + Mn_2O_3(s, I_{A\bar{3}}) \xrightarrow{reaction} 2LiMn_2O_4(s, F_{d\bar{3}m})} \quad (13)$$

$$\mathrm{2MnO_2\left(s, P_{42/mnm}\right) \xrightarrow{reaction} Mn_2O_4(s, F_{d\bar{3}m})} \quad (14)$$

In a word, when the Gibbs free energies of a reaction ($\Delta_r G_{\mathrm{m}}$) was obtained, the molar Gibbs formation energies ($\Delta_f G_{\mathrm{m,el.}}$) of the cathode materials ***from element phases*** can be determined. The computational results were summarized in Table 2.

(2) Gibbs free energy of relevant decomposition reactions ($\Delta_r G_{\mathrm{m,ox.}}$).

As a negative Gibbs formation energy relative to elemental phases is not sufficient to prove that a material is thermodynamically stable [4,5], the Gibbs free energies of some relevant decomposition reactions were also introduced. Furthermore, to compare with the available experimental data[1-3], ***we have rewritten the decomposition reactions in a reverse manner***. For $LiMPO_4$ and MPO_4 compounds, the reactions were,

$$\mathrm{Li_2O(s, F_{m\bar{3}m}) + 2FeO(s, F_{m\bar{3}m}) + P_2O_5(s, P_{nma}) \xrightarrow{reaction} 2LiFePO_4(s, P_{nma})} \quad (15)$$

$$\mathrm{Li_2O(s, F_{m\bar{3}m}) + 2MnO(s, F_{m\bar{3}m}) + P_2O_5(s, P_{nma}) \xrightarrow{reaction} 2LiMnPO_4(s, P_{nma})} \quad (16)$$

$$2\mathrm{FeO}(\mathrm{s}, F_{m\bar{3}m}) + \mathrm{P_2O_5}(\mathrm{s}, P_{nma}) + \frac{1}{2}O_2(g) \xrightarrow{reaction} 2\mathrm{FePO_4}(\mathrm{s}, P_{nma}) \quad (17)$$

$$2\mathrm{MnO}(\mathrm{s}, F_{m\bar{3}m}) + \mathrm{P_2O_5}(\mathrm{s}, P_{nma}) + \frac{1}{2}O_2(g) \xrightarrow{reaction} 2\mathrm{MnPO_4}(\mathrm{s}, P_{nma}) \quad (18)$$

For $LiMO_2$ ($R_{\bar{3}m}$), MO_2 ($R_{\bar{3}m}$), $LiMn_2O_4$ ($F_{d\bar{3}m}$), and Mn_2O_4 ($F_{d\bar{3}m}$) electrode materials, the experimental reaction pathways (Eq.(9)~Eq.(14)) were also used.

It should be noted that the Gibbs free energies of relevant reactions ($\Delta_r G_m$, Eq. (9) to Eq. (18)) actually correspond to the Gibbs formation energies of cathode compounds ***from relevant oxides*** ($\Delta_f G_{m,ox.}$). If one would like to analyze the thermodynamic stabilities of cathode materials, then the reaction free energies for relevant decomposition reactions obtained by replacing the values above with a negative sign ("-") should be used. Table S1 listed the experimental formation enthalpies, Gibbs formation energies, and our calculated total energies of relevant compounds, from which the quantities listed in Table 2 can be derived.

(3) Other possible decomposition products and reactions.

As suggested by the experimental data in Table S1, M_2O_3 and M_3O_4 are much more stable than MO. It seems that the calculated reaction free energies would change from positive to negative when the more stable decomposition products were chosen, and the decomposition reactions became spontaneous.

However, this assumption is not always correct due to the ***stoichiometry restriction of a reaction***. By taking M_2O_3 as an example, we can construct the following reaction,

$$2\mathrm{Li}(\mathrm{s}, F_{m\bar{3}m}) + \mathrm{M_2O_3}(\mathrm{s}) + \mathrm{P_2O_5}(\mathrm{s}, P_{nma}) \xrightarrow{reaction} 2\mathrm{LiMPO_4}(\mathrm{s}, P_{nma}) \quad (19)$$

According to the data listed in Table S1, the reaction free energies are calculated to be -481.282 and -491.939 kJ·mol^{-1} for $LiFePO_4$ and $LiMnPO_4$ respectively. The results indicated that $LiMPO_4$ is more difficult to decompose into M_2O_3 when comparing with the MO case. Such a phenomenon is not difficult to understand, because Eq. (19) can be combined with Eq. (20) to form Eq. (21),

$$\mathrm{Li_2O}(\mathrm{s}, F_{m\bar{3}m}) + 2\mathrm{MO}(\mathrm{s}, F_{m\bar{3}m}) + \mathrm{P_2O_5}(\mathrm{s}, P_{nma}) \xrightarrow{reaction} 2\mathrm{LiMPO_4}(\mathrm{s}, P_{nma}) \quad (20)$$

$$2\mathrm{Li}(\mathrm{s}, F_{m\bar{3}m}) + \mathrm{M_2O_3(s)} \xrightarrow{reaction} \mathrm{Li_2O}(\mathrm{s}, F_{m\bar{3}m}) + 2\mathrm{MO}(\mathrm{s}, F_{m\bar{3}m}) \quad (21)$$

Although M_2O_3 is much more stable than MO, the total free energy of the right-hand side of Eq. (21) is actually more negative than that of the left-hand side one. Therefore, $LMPO_4$ trends to be decomposed into MO and Li_2O rather than lithium and M_2O_3. Similarly, when M_3O_4 was considered, the reaction can be revised to,

$$2\mathrm{Li(s)} + 0.5\mathrm{Li_2O}(s) + \mathrm{M_3O_4(s)} + 1.5\ \mathrm{P_2O_5(s)} \xrightarrow{reaction} 3\mathrm{LiMPO_4(s)} \quad (22)$$

The calculated reaction free energies for the $LiFePO_4$ and $LiMnPO_4$ cases were about -459.714 and -487.111 kJ·mol^{-1}, respectively. Therefore, $LiMPO_4$ is still preferred to decompose into MO rather than M_3O_4. The combination of Eq. (21) and Eq. (22) produces Eq. (23), which makes the reason obvious.

$$2\mathrm{Li}(\mathrm{s}, F_{m\bar{3}m}) + \mathrm{M_3O_4(s)} \xrightarrow{reaction} \mathrm{Li_2O}(\mathrm{s}, F_{m\bar{3}m}) + 3\mathrm{MO}(\mathrm{s}, F_{m\bar{3}m}) \quad (23)$$

When the rodolicoite products were considered, the reaction can be revised to,

$$\mathrm{Li}(\mathrm{s}, F_{m\bar{3}m}) + \mathrm{MPO_4(s)} \xrightarrow{reaction} \mathrm{LiMPO_4}(\mathrm{s}, P_{nma}) \quad (24)$$

It should be pointed out that only one structure for $MnPO_4$ can be found and its symmetry (P_{nma}) is identical to that of $LiMnPO_4$ compound. In this case, only $LiFePO_4$ should be considered, and the reaction free energy is about -384.864 kJ·mol^{-1}. As the free energies of the decomposition reactions mentioned above are all higher (absolute value) than the values for the MO case, MO is thus chosen to be the decomposition product. Moreover, for the delithiated states, additional decomposition reactions were also considered,

$$\mathrm{M_2O_3(s)} + \mathrm{P_2O_5}(\mathrm{s}, P_{nma}) \xrightarrow{reaction} 2\mathrm{MPO_4}(\mathrm{s}, P_{nma}) \quad (25)$$

$$\mathrm{M_3O_4(s)} + 1.5\ \mathrm{P_2O_5}(\mathrm{s}, P_{nma}) + 0.25\ \mathrm{O_2}(g) \xrightarrow{reaction} 2\mathrm{MPO_4}(\mathrm{s}, P_{nma}) \quad (26)$$

The calculated reaction free energies of Eq. (25) are about -142.052 and -103.413 kJ·mol^{-1} for $FePO_4$ and $MnPO_4$ respectively, while the values of Eq. (26) are -218.609 and -196.710 kJ·mol^{-1}. Therefore, delithiated state MPO_4 trends to be decomposed into M_2O_3 rather than MO or M_3O_4.

References:

(1) Wang, M.; Navrotsky, A., *J. Solid State Chem*, **2005**,178, 1230-1240.

(2) Wang, M.; Navrotsky, A., *Solid State Ionics* **2004**, *166*, 167-173.

(3) Wang, M.; Navrotsky, A., *J. Solid State Chem.* **2005**, *178*, 1182-1189.

(4) Ong, S. P.; Mo, Y. F.; Richards, W. D.; Lee, H. S.; Ceder, G., *Energy Environ. Sci.* **2013**, 6, 148-156.

(5) Ong, S. P.; Wang, L.; Kang, B.; Ceder, G., *Chem. Mater.* **2008**, 20, 1798-1807.

(6) Barin, I., Thermochemical Data of Pure Substances (3rd Edition), Wiley-VCH Verlag GmbH, Weinheim, Germany, 1995.

Table S1 Experimental formation enthalpies, Gibbs formation energies, and calculated total energies of relevant compounds.

Compd.	Sym.	$\Delta_f H_m$ (kJ·mol^{-1}) [a]	$\Delta_f G_m$ (kJ·mol^{-1}) [a]	Total Energies (eV)
Li	$I_{m\bar{3}m}$	0.000	0.000	-190.19897
Mn	$F_{m\bar{3}m}$	0.000	0.000	-655.20625
Fe	$I_{m\bar{3}m}$	0.000	0.000	-867.28118
Li_2O	$F_{m\bar{3}m}$	-598.730	-562.104	-821.04953
FeO	$F_{m\bar{3}m}$	-272.044	-251.441	-1302.64440
Fe_2O_3	$R_{\bar{3}c}$	-824.248	-742.294	-3041.92398
Fe_3O_4	$F_{d\bar{3}m}$	-1118.383	-1015.227	-4343.23076
MnO	$F_{m\bar{3}m}$	-385.221	-362.898	-1092.04591
MnO_2	$P_{42/mnm}$	-520.029	-465.138	-1525.02246
Mn_2O_3	$I_{A\bar{3}}$	-959.002	-881.114	-2620.71916
Mn_3O_4	$I_{41/AMD}$	-1387.799	-1283.232	-3710.90307
CoO	$F_{m\bar{3}m}$	-237.944	-214.198	-1479.63688
NiO	$F_{m\bar{3}m}$	-239.701	-211.539	-1791.92028
P_2O_5	P_{nma}	–	–	-2550.23523
O_2	–	0.000	0.000	-869.09653
$FePO_4$	P_{3121}	-1297.500	-1184.607	-2797.07886
$LiFePO_4$	P_{nma}	–	–	-2991.26647
$FePO_4$	P_{nma}	–	–	-2797.55180
$LiMnPO_4$	P_{nma}	–	–	-2780.77451
$MnPO_4$	P_{nma}	–	–	-2586.54894
$LiCoO_2$	$R_{\bar{3}m}$	–	–	-2108.82026
CoO_2	$R_{\bar{3}m}$	–	–	-1914.43739
$LiNiO_2$	$R_{\bar{3}m}$	–	–	-2420.22535
NiO_2	$R_{\bar{3}m}$	–	–	-2225.91495
$LiMn_2O_4$	$F_{d\bar{3}m}$	–	–	-3248.26733

Mn_2O_4	$F_{d\bar{3}m}$	–	–	-3053.88401

[a] Standard state experimental data are taken from Ref. [6]

(4) Reaction free energies for $2MPO_4$ -> $M_2P_2O_7$ + $0.5O_2$.

As the decomposition reaction, $2MnPO_4$ -> $Mn_2P_2O_7$ + $0.5O_2$, was reported in literature, to provide some relevant information we also evaluated the corresponding reaction free energies. The values were listed in Table S2. The results indicated that the decomposition reaction from $MnPO_4$ to $Mn_2P_2O_7$ is endothermic, and the counterpart reaction for $FePO_4$ compound is more difficult to occur, which is well consistent with experimental findings.

Table S2 Relevant quantities for reaction $2MPO_4$ -> $M_2P_2O_7$ + $0.5O_2$.

	$E(MPO_4)$ (eV)	$E(M_2P_2O_4)$ (eV)	$E(O_2)$ (eV)	$S^o(O_2)$ (J/mol) [a]	$\Delta_r G_m$ ($kJ \cdot mol^{-1}$)
$FePO_4$ (P_{nma})	-2797.5518	-5156.2659	-869.0965	205.15	206.89
$MnPO_4$ (P_{nma})	-2586.5489	-4735.3909	-869.0965	205.15	152.34

[a] standard entropy for gas phase O_2 taken from NIST chemistry webbook (http://webbook.nist.gov/).

Algorithms for calculating the mechanical properties

(1) Stress-Strain relationship.

For each material, both stress and strain have three tensile and three shear components, giving six components in total. According to the theory of elasticity, a 6×6 symmetric matrix with 36 elements is thus needed to describe the relationship between stress and strain. Thanks to the symmetries, the independent elastic constants are reduced to 9 values for orthorhombic crystals. Therefore, the strain dependence of stress can be expressed as

$$\begin{pmatrix} \sigma_{xx} \\ \sigma_{yy} \\ \sigma_{zz} \\ \tau_{yz} \\ \tau_{zx} \\ \tau_{xy} \end{pmatrix} = \begin{pmatrix} C_{11} & C_{12} & C_{13} & 0 & 0 & 0 \\ C_{21} & C_{22} & C_{23} & 0 & 0 & 0 \\ C_{31} & C_{32} & C_{33} & 0 & 0 & 0 \\ 0 & 0 & 0 & C_{44} & 0 & 0 \\ 0 & 0 & 0 & 0 & C_{55} & 0 \\ 0 & 0 & 0 & 0 & 0 & C_{66} \end{pmatrix} \begin{pmatrix} \varepsilon_{xx} \\ \varepsilon_{yy} \\ \varepsilon_{zz} \\ \gamma_{yz} \\ \gamma_{zx} \\ \gamma_{xy} \end{pmatrix} \quad (27)$$

where σ is tensile stress, τ the shear stress, ε the tensile strain, and γ the shear strain. C_{ij} (i = 1, 6; j = 1,6) are elastic constant matrix elements and they are related to the compliance (S_{ij}) matrix elements by $S = C^{-1}$.

(2) Mechanical stability criterion.

Born and Huang [7] have systematically investigated the lattice mechanical stability and formulated the stability criteria in terms of the elastic constants C_{ij}, and they pointed out that the criterion for a mechanically stable lattice requires that the elastic energy density be a positive definite quadratic function of strain. For orthorhombic crystals, the criterions are [8,9]

$$C_{11}+C_{22}+C_{33}+2C_{12}+2C_{13}+2C_{23}>0 \quad (28)$$

$$C_{11}+C_{33}-2C_{13}>0 \quad (29)$$

$$C_{11}+C_{22}-2C_{12}>0 \quad (30)$$

$$C_{22}+C_{33}-2C_{23}>0 \quad (31)$$

$$C_{ij}\,(i=j)>0 \quad (32)$$

(3) Methods for evaluating the polycrystalline modulus.

To obtain a reasonable result, the moduli for polycrystalline materials should be used in the present case. There are two approximation methods to calculate the polycrystalline modulus, namely, the Voigt scheme and the Reuss one. For orthorhombic crystals, the shear modulus (G) and the bulk modulus (B) according to Reuss (subscripts R) and Voigt (subscripts V) approximations are given by,

$$\frac{1}{G_R}=\frac{4}{15}\left(S_{11}+S_{22}+S_{33}\right)-\frac{4}{15}\left(S_{12}+S_{13}+S_{23}\right)+\frac{3}{15}\left(S_{44}+S_{55}+S_{66}\right) \quad (33)$$

$$G_V=\frac{1}{15}\left(C_{11}+C_{22}+C_{33}-C_{12}-C_{13}-C_{23}\right)+\frac{1}{5}\left(C_{44}+C_{55}+C_{66}\right) \quad (34)$$

and

$$\frac{1}{B_R}=\left(S_{11}+S_{22}+S_{33}\right)+2\left(S_{12}+S_{13}+S_{23}\right) \quad (35)$$

$$B_V=\frac{1}{9}\left(C_{11}+C_{22}+C_{33}\right)+\frac{2}{9}\left(C_{12}+C_{13}+C_{23}\right) \quad (36)$$

References:

(7) Born, M.; Huang, K., Dynamical Theory of Crystal Lattices, Oxford: Oxford University Press,1998.

(8) Jiang, C.; Srinivasan, S. G.; Caro, A.; Maloy, S. A., *J. Appl. Phys.* **2008**, *103*, 043502.

(9) Koc, H.; Mamedov, Amirullah M.; Deligoz, E.; Ozisik, H., *Solid State Sci.* **2012**, *14*, 1211-1220.

Correlation between shear deformation and chemical bonds

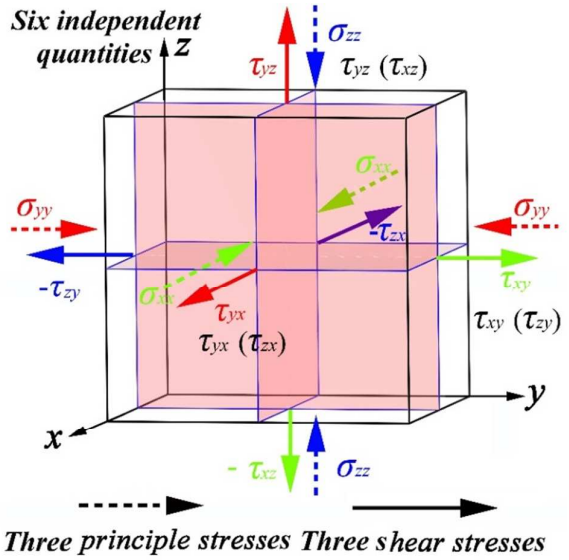

Figure S1 Materials under stresses.

Figure S1 showed the material under stresses. When the principle stress is applied, two shear stresses that are perpendicular to the normal stress appear. As a result, the material will suffer from strains and deformations. Principle strain and deformation will occur along the normal direction, while shear stain and deformation will happen along the shear direction. C_{11}, C_{22}, and C_{33} are directly related to *a*, *b*, and *c* directional resistance of materials against uniaxial tension, while C_{44}, C_{55}, and C_{66} measure the shear resistance of materials regarding the {100},{010}, and {001} crystal planes against shear tensions.

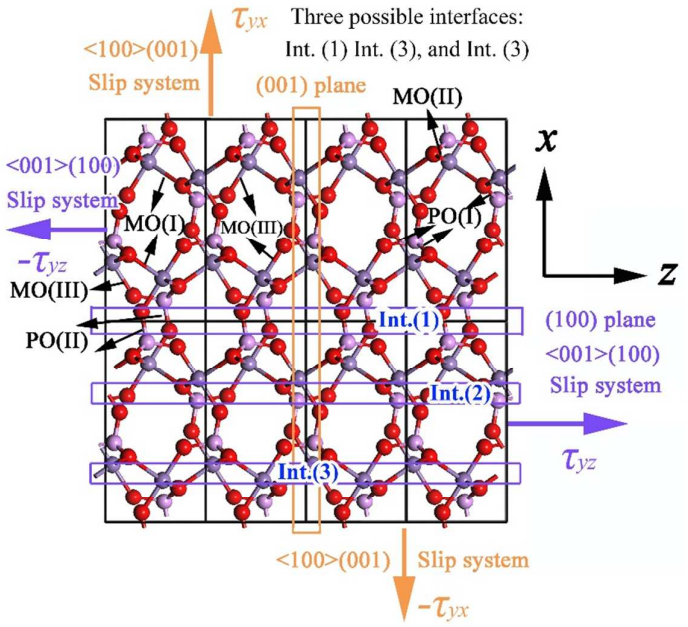

Figure S2 Scheme for the shear deformations within the xoz plane.

Figure S2 showed the projection of the Li_xMPO_4 materials into the xoz plane. When the principle stress (σ_{yy}) was applied along the y axis, principle deformation will occur along the [010] direction. At the same time, τ_{yz} and τ_{yx} will appear within the xoz plane, leading to the corresponding shear deformations. The shear deformation can be defined as the parallel movement of two parallel cross sections of the material. It is known that C_{44} is associated with τ_{yz} and γ_{yz} ($\tau_{yz}=C_{44}\cdot\gamma_{yz}$). When the shear stain occurs, the most active (100) interface is the one with the weakest bonding, and the shear deformation related to this (100) interface will be more energetically favorable. Figure S2 showed three possible (100) interfaces. To determine which one is the weakest, the total bond population per unit cell is calculated and the results were listed in Table S3.

It can be found that the third interface labeled as Int. (3) is the weakest. For a given plane the weakest chemical bond will play a dominant role. As a result, the shear deformation related to C_{44} and the (100) plane of Li_xMPO_4 compounds will be determined by the weakest M-O(I) bond. This deduction can also be supported by the

following fact. After Li^+ extraction, the total bond population of Int. (3) for $FePO_4$ increases, while the value for $MnPO_4$ is almost the same. However, the Mn-O(I) bond strength is weakened obviously (0.12 *vs*. 0.08), while the Fe-O(I) bond is nearly unchanged (0.12 *vs*. 0.13), which well explains why C_{44} of $MnPO_4$ decreases significantly.

Table S3 Total bond populations for different interfaces of Li_xMPO_4 compounds.

	no.	Chemical bonds	$LiFePO_4$	$FePO_4$	$LiMnPO_4$	$MnPO_4$
C_{44} (100)	Int. (1)	2 P-O(II)	1.32	1.32	1.30	1.30
	Int. (2)	2 P-O(I), 2 M-O(III)	1.70	1.84	1.70	1.91
	Int. (3)	4 M-O(I), 2 M-O(III)	0.98	1.18	0.98	1.02
C_{55} (010)	Int. (1)	4 M-O(II)	1.12	0.92	1.04	1.16
	Int. (2)	2 PO(I), 2 M-O(I), 2 M-O(II)	2.00	1.90	2.12	1.96
C_{66} (001)	Int. (1)	2 P-O(II), 2 M-O(III) 4 M-O(I)	2.30	2.50	2.28	2.32
	Int. (2)	1 P-O(II), 2 P-O(II) 2 M-O(I), 2 M-O(II) 1 M-O(III)	2.91	2.89	2.86	2.96
	Int. (3)	4 M-O(I), 2 M-O(III)	0.98	1.18	0.98	1.02

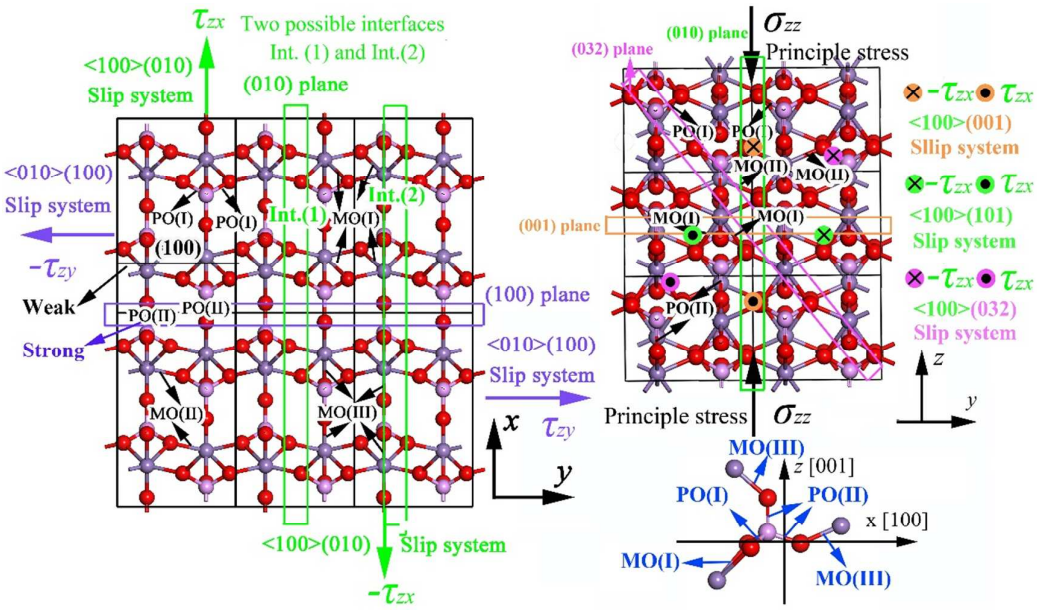

Figure S3 Scheme for the shear deformations related to τ_{zx}.

C_{55} is associated with τ_{zx} and γ_{zx} (τ_{zx}=C_{55}·γ_{zx}), and the corresponding shear deformation is related to the (010) plane. As showed in Figure S3, there are two possibilities, and the (010) plane is either across the M-O(II) bonds or across the M-O(I),M-O(II), and P-O(I) bonds. The total bond populations per unit cell for the former and the later cases are about 1.12 and 2.00 for $LiFePO_4$, respectively. Therefore, the shear deformation concerning the former (100) plane is preferable, and the M-O(II) bonds are thus responsible for the C_{55} values of Li_xMPO_4 compounds. The right panel of Figure S3 also showed some slip systems relevant to τ_{zx}. However, as there is no interface that is weaker than Int. (1), the shear deformation related to τ_{zx} and γ_{zx} is thus restricted within the (010) plane.

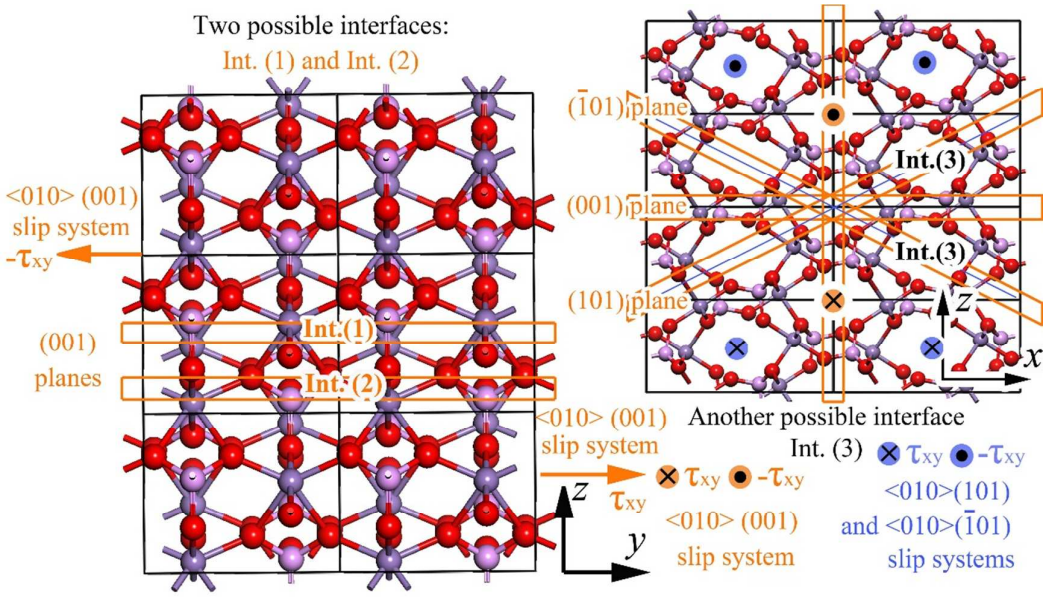

Figure S4 Scheme for the shear deformations related to τ_{xy}.

Figure S4 showed the shear deformations related to τ_{xy} and γ_{xy} ($\tau_{xy}=C_{66}\cdot\gamma_{xy}$). There are two possibilities within the zoy plane. The total bond populations for the former and the later interfaces are calculated to be 2.30 and 2.91 for $LiFePO_4$. It is expected that the resistance of the materials against shear strain and deformation would be rather strong. However, the calculated C_{66} of Li_xMPO_4 is actually small. Such an abnormality is elusive. To clarify this problem, other possibilities were considered. As illustrated in the right panel of Figure S4, two interfaces ((101) and $(\bar{1}01)$) are found, and the total bond populations (4 M-O(I) and 2 M-O(II) bonds) for them are both 0.98 for $LiFePO_4$, which indicated that the interfaces are much weaker. Therefore, the shear deformation concerning these two planes is energetically favorable. Furthermore, as M-O(I) bond is much weaker than M-O(II) one, it thus responsible for the small value of C_{66}. After Li^+ extraction, the Mn-O(I) bond strength is further weakened, leading to the obvious decrease of C_{66} in $MnPO_4$. While the nearly unchanged Fe-O(I) bond of $FePO_4$ results in a very similar C_{66}.